Toward a Rational Design of Titanium Metal-Organic Frameworks

Sujing Wang, Helge Reinsch, Nicolas Heymans, Mohammad Wahiduzzaman, Charlotte Martineau-Corcos, Guy de Weireld, Guillaume Maurin, Christian Serre

▶ **To cite this version:**

Sujing Wang, Helge Reinsch, Nicolas Heymans, Mohammad Wahiduzzaman, Charlotte Martineau-Corcos, et al.. Toward a Rational Design of Titanium Metal-Organic Frameworks. Condensed Matter, 2020, 2 (2), pp.440-450. 10.1016/j.matt.2019.11.002 . hal-02900073

HAL Id: hal-02900073
https://hal.science/hal-02900073

Submitted on 25 May 2021

HAL is a multi-disciplinary open access archive for the deposit and dissemination of scientific research documents, whether they are published or not. The documents may come from teaching and research institutions in France or abroad, or from public or private research centers.

L'archive ouverte pluridisciplinaire **HAL**, est destinée au dépôt et à la diffusion de documents scientifiques de niveau recherche, publiés ou non, émanant des établissements d'enseignement et de recherche français ou étrangers, des laboratoires publics ou privés.

Toward a Rational Design of Titanium Metal-Organic Frameworks

Sujing Wang[1,2,8*], Helge Reinsch[3], Nicolas Heymans[4], Mohammad Wahiduzzaman[5], Charlotte Martineau-Corcos[6,7], Guy De Weireld[4], Guillaume Maurin[5], Christian Serre[1*]

[1]Institut des Matériaux Poreux de Paris, UMR 8004 CNRS, Ecole Normale Supérieure, Ecole Supérieure de Physique et de Chimie Industrielles de Paris, PSL Université, 75005 Paris, France.

[2]Hefei National Laboratory for Physical Sciences at the Microscale, University of Science and Technology of China, 230026 Hefei, China

[3]Institut für Anorganische Chemie, Christian-Albrechts-Universität Kiel, 24118, Kiel, Germany

[4]Laboratoire de Thermodynamique et Physique mathématique, Faculté Polytechnique de Mons, Université de Mons, 20 Place du Parc, 7000 Mons, Belgium

[5]Institut Charles Gerhardt, Montpellier UMR 5253 CNRS ENSCM UM, Université Montpellier, Place Eugène Bataillon, 34095 Montpellier cedex 05, France.

[6]Institut Lavoisier de Versailles, UMR 8180 CNRS, Université de Versailles Saint-Quentin-en-Yvelines, Université Paris-Saclay, 78035 Versailles, France.

[7]CEMHTI, UPR 3079 CNRS, 45071 Orléans CEDEX 2, France

[8]Lead Contact

Correspondence: sjwang4@ustc.edu.cn

christian.serre@ens.fr

SUMMARY

The complexity of Ti-chemistry in solution not only leads to the difficulty of isolating crystalline titanium metal-organic frameworks (Ti-MOFs), but also brings the challenge of controlled assembly of the crystal structure. We report here the first example of a controlled synthesis of a Ti-MOF structure through a linker exchange strategy directly from a pre-formed Ti-O cluster. A Ti_8O_8 cluster precursor with terminal formate and acetate ligands (Ti_8AF) was reacted with trimesic acid (BTC) under green and mild conditions, generating a microporous Ti-MOF (MIP-207) while preserving the connection and configuration of the Ti_8O_8 core. In addition, due to the ditopic *meta*-positional connection mode of the linker, the chemical environment and functionality of the structural voids could be easily tuned by substituting trimesate moieties with isophthalate type linkers via concise one-pot reactions. This finally resulted in an adjustable performance in CO_2 capture over N_2.

INTRODUCTION

Titanium metal-organic frameworks (Ti-MOFs) have attracted considerable and continuous attention over the past decade, mainly due to the low toxicity and rich natural abundance of titanium element, the well-recognized specialty of Ti-MOFs in photocatalysis,[1-4] as well as their great promises in gas separation.[5; 6] However, the complexity of Ti-chemistry in solution has led so far to notable difficulties in controlling the Ti-MOFs structures. For all the published Ti-MOFs obtained from direct synthesis using simple Ti precursors, including MIL-91,[7] MIL-125,[8] NTU-9,[9] MIL-101,[10] COK-69,[11] Ti-CAT-5,[12] MIL-167,[13] MIP-177,[14] MIL-100,[15] Ti-TBP,[16] and ZSTUs,[17] their inorganic building units range from discrete Ti-O clusters to infinite chains, showing the highly unpredictable feature of Ti reaction. In this regard, only post-synthetic cation exchange between MOFs built with various metal centers of known secondary building units (SBUs) and Ti ions has led to Ti-MOFs in a structure controlled manner.[18-20]

In order to achieve a better structure control of the resulting MOF during direct synthesis, Zhou and co-workers firstly tried to prepare PCN-22 in DEF/benzoic acid under solvothermal condition involving a pre-formed Ti_6 cluster compound as precursor, which efficiently slowed down the crystallization and thus gave rise to single crystal product.[21] Nonetheless, a break of the pristine Ti_6 cluster and its re-organization into a Ti_7 one was revealed by single crystal structure analysis. Later, using the same Ti_6 cluster complex in methanol, an exciting progress of synthesizing Ti-MOF over control was achieved by Yaghi and co-workers applying a combined MOF and COF strategy. MOF-901 was successfully assembled via the imine formation from the amino group of the Ti_6 cluster protecting ligand and the aldehyde groups of the organic spacer, during which the connection of the Ti_6 cluster core was not disturbed.[22] This method was proven to tolerate other di-aldehydes spacers by the preparation of MOF-902, which represents the first example of reticular chemistry in Ti-MOFs.[23] The challenge remained here is to realize the controlled formation of Ti-MOF by modulating the Ti-O coordination bond of the cluster instead of the organic covalent bonds from the protective ligand, as the cases reported before for the other metal based MOFs, such as Fe[24-26] and Zr[27-29] ones.

Very recently, DGIST-1 was reported by Park and co-workers, which displays an infinite Ti-O chain inorganic building block resulting from the reorganization of the pristine Ti_6 or Ti_8 clusters in DEF/benzoic acid reaction system.[30] Similarly, Lin and co-workers found that a Ti_3 building unit was generated in DMF/acetic acid mixture when the same Ti_6 cluster precursor reacted with BPDC linker.[31] It further supported that alternative solvent systems other than the conventional one, i.e. DEF or DMF with modulators, could be an important factor to help the preservation of the original connectivity in the Ti-O cluster precursor during reactions.

In addition, the configuration of the Ti-O cluster precursor, such as the chemical component and connection mode, could be another essential determinant for the linker exchange process during the MOF framework formation. All the aforementioned Ti-O clusters reported so far feature large terminal mono-carboxylate ligands with bulky aromatic moieties in a dense arrangement configuration, which could possibly impede the effective bonding exchange between the protective species and the targeting linker for MOF formation. In this case, Ti-O connections of the cluster have to be reorganized to preferentially facilitate the linker exchange. Therefore, selection of a Ti-O cluster precursor with adequate space flexibility, particularly protected by small and appropriate terminal ligands such as formate or acetate, could be a feasible solution. However, to our knowledge, controlled synthesis of Ti-MOF starting from such Ti-O clusters with adapted reactivity and directly via linker exchange has never been achieved so far.

Herein, we report a controlled preparation of a microporous Ti-MOF, denoted as MIP-207 (MIP stands for the Materials of the Institute of porous materials from Paris), via direct ligand exchange between the small terminal mono-carboxylate species of a Ti_8O_8 cluster (Ti_8-acetate-formate, Ti_8AF) and the targeting trimesic acid for MOF fabrication. MIP-207 could be synthesized not only under solvothermal condition by using the pre-formed Ti_8 cluster as precursor, but also in reflux reaction under ambient pressure by the assembly of the *in situ* generated Ti_8O_8 cluster and trimesic acid, which is concise and facile for scale-up preparation. The BTC linker in the structure adopts a *meta*-connection mode leaving the free carboxylic group pointing towards the pore, which allows a successful partial substitution of trimesate linker by different isophthalates with

diverse functional groups, so that the chemical environment of the MOF pore could be tuned. It is noteworthy that the Ti_8AF cluster features an appropriate reactivity and a green scalable production, which makes it a suitable precursor for rational design and direct syntheses of Ti-MOFs. Furthermore, MIP-207 displays a good water stability at room temperature, a promising adsorptive selectivity of carbon dioxide (CO_2) over nitrogen suitable for future CO_2 working adsorption processes.

RESULTS AND DISCUSSION

Considerable progress of crystalline Ti-O clusters has been achieved during the past few decades, leading to diverse structures with different number of Ti centers.[32-36] In most cases, the syntheses of Ti-O clusters require hydrolysis of Ti precursor under solvothermal conditions, which is always limited by long reaction time, low reaction yield and small scale for further applications. In contrast, the Ti_8AF cluster was prepared under reflux condition with ambient pressure for a short duration, simply heating the mixture of $Ti(iPrO)_4$, formic acid and acetic anhydride in round bottom flask in contact with air. This facile process allows an easy scale-up preparation.

The crystal structure of $Ti_8(\mu_2\text{-}O)_8(acetate)_{12}(formate)_4$ (Ti_8AF) cluster was solved *ab initio* from high resolution powder X-ray diffraction (PXRD) data (Figure S1 and S2, Table S1 and S2). As shown in Figure 1, different from the reported Ti_8 clusters, the protective ligands of the Ti_8AF cluster are bridging formates and acetates, which are of much less steric hindrance or weaker bonding interactions with the Ti(IV) ions in comparison with those reported, such as 4-aminobenzoic acid, terephthalic acid, isobutyric acid, sulfate, to quote a few. It not only provides adequate space and freedom for the coordination surrounding but also possesses an appropriate coordination strength between the ligands and Ti-O core, as it is well demonstrated that both formate and acetate are good modulators for MOF synthesis and thus replaced by multi-topic carboxylate linkers smoothly.[37-39] Hence a much easier installation of the MOF linker molecule could be promoted via an efficient linkage exchange when the Ti_8AF cluster is used as precursor (See Figure S6-S9 for the detailed characterizations).

With the Ti_8AF cluster in hand, controlled synthesis of Ti-MOF using it as precursor was carried out. Based on the influence of the reported solvent systems, acetic anhydride

was selected since it is a widely used solvent in organic synthesis and it has been proven to be efficient for MOF preparation.[40] A highly crystalline Ti-MOF of chemical formula $Ti_8(\mu_2\text{-}O)_8(acetate)_8(BTC)_4$, named MIP-207, was obtained in the solvent mixture of formic acid and acetic anhydride under solvothermal condition (Figure S10). Crystal structure was initially solved from PXRD data and further refined with the geometry optimization performed at the DFT level (Table S3, S4; Figure S3-S5). It reveals that MIP-207 structure crystallizes in a tetragonal *P*4/nbm space group with unit-cell parameters of $a=b=24.2224(15)$ Å, $c=7.8291(5)$ Å, $V=4593.5(6)$ Å^3. As shown in Figure 2a, the entire arrangement and configuration of the Ti_8 cluster core is maintained in the SBU of MIP-207. A thorough ligand exchange was observed for all the terminal formates. Eight carboxylate groups from the BTC molecules occupy the adjacent positions of formates and acetates in an up and down mode above and below the symmetrical plane of the cluster core, which could be due to the steric hindrance repulsion effect. Each Ti_8 cluster is interconnected with neighboring four SBUs by using a *meta*-position carboxylate group of the BTC linker, forming a 2D layer with a large amount of free carboxylic acid groups facing the voids (Figure 2b). The presence of both acetate and BTC moieties is confirmed by the ^{13}C solid-state NMR spectrum (Figure S13, S14), in which all carboxylic carbon atoms are clearly distinguished. The presence of the free carboxylic groups is validated by the ^1H solid-state NMR spectrum that displays a characteristic acidic proton at 13.3 ppm (Figure S13). Contiguous layers stack to each other in a strictly ordered fashion so that the channel of about 6 Å (Figure S12) inside the Ti_8 cluster and between SBUs are kept when viewed along the *c*-axis of the structure (Figure 2c), resulting in a Brunauer–Emmett–Teller (BET) area of 570 $m^2\ g^{-1}$ and a free pore volume of 0.34 $cm^3\ g^{-1}$ deduced from the nitrogen porosimetry data collected at 77 K (Figure S11, Table S5). There is a considerable amount of guest water molecules accommodated between layers, supplying intermolecular hydrogen bonding for guest-guest and guest-host interactions to further stabilize the crystal structure of MIP-207 (Figure 2d).

Since the Ti_8AF cluster and MIP-207 share the same solvent system for preparation, a direct synthesis using $Ti(iPrO)_4$ as the Ti(IV) precursor was considered. As expected, MIP-207 was obtained from heating the mixture of $Ti(iPrO)_4$ and BTC in the presence of

formic acid and acetic anhydride under solvothermal condition. A further attempt of performing the same reaction under reflux condition worked as well however with a slightly less crystalline product. Additionally, the absence of formate in the MIP-207 structure inspired us to replace formic acid by acetic acid, since acetic acid is much more cost-effective and of less risk when handled with a large quantity in comparison with formic acid. To this end, a product of the same phase but with a slightly worse crystallinity was obtained applying acetic acid instead of formic acid. Thus the preparation of MIP-207 was improved to a green scalable chemistry level, which could be of remarkable benefit for its future applications at an industrial scale.

Water stability is an important concern for MOFs when real application conditions are considered. Therefore, stability of MIP-207 in contact with water was checked (Figure S15). First, a long time (18 months) exposure of MOF sample in open air atmosphere was carried out. The PXRD pattern of the corresponding product did not show obvious change in comparison with that of the pristine compound, suggesting a good stability of MIP-207 in air at room temperature. Similar observation was noticed when the MOF sample was soaked in water for three days at room temperature. Nevertheless, MIP-207 displays limited hydrothermal resistance, which is similar to other reported Ti-MOFs. Both hot water vapor (100°C) and hot liquid water (80°C) could destruct the long-range order of MIP-207 crystal structure within 24 hours. Therefore, MIP-207 presents a moderate water stability as the same level of NH_2-MIL-125, which is adequate for applications involving water vapor at low temperatures.[14; 41; 42]

Thermal stability of MIP-207 was evaluated by a combined analysis of thermogravimetric data and temperature-dependent PXRD data (Figure S16 and S17). A continuous weight loss was observed from room temperature to 325°C in the TGA curve before the sharp drop, which could be ascribed to the gradual departure of guest solvent molecules and terminal acetates. The PXRD patterns confirm the well-maintaining of the long-range order of the MOF crystal structure up to 300°C, with slight alterations in relative intensity of some peaks. Further increase of heating temperature leads to a fast decomposition of the MOF structure, evidenced by a steep weight loss in

TGA and a significant decrease of crystallinity in PXRD. Therefore, MIP-207 is among the best thermally stable Ti-MOFs reported so far.

The BTC molecule in the MIP-207 structure uses two carboxylate groups at *meta*-positions on the benzene ring for the linkage of SBUs and leaves the third carboxylic acid group free from coordination; thus it could be considered as an isophthalate type linker. Thus, in order to make the chemical environment of the MOF cavity diverse and tunable, we can envisage partial or even entire replacement of the BTC by other functional linkers with similar molecular size and angles between the two connection sites as that of the isophthalic acid (IPA). Accordingly, various similar linkers have therefore been tested under the same reaction condition (acetic acid/acetic anhydride solvent system, reflux) and the corresponding results are shown in Figure 3 and listed in Table 1.

If no crystalline MOF comprising the pure isopthalate ligands could be obtained, a good tolerance towards a large range of functional groups of this substitution reaction was observed when partial substitution of trimesate by IPA derivatives was applied (Table 1, entries 2-12; Figure S18-S21). Interestingly, the electronic effect of the functional group plays an important role in determining the final ratio of the secondary linker included. Compared to the electron-withdrawing free carboxyl group in the pure MIP-207 structure, the electron-donating functions including H, Me, OH, NH_2, OMe and tBu on the IPA moiety all result in replacing ratios below 10% (Table 1, entries 2-7; Figure S22). In a sharp contrast, electron-withdrawing functional groups, such as -NO_2, -SO_3H, -F, -Br and pyridyl (Table 1, entries 8-12; Figure S23), give rise to elevated substitution proportions (i.e. 12-18 mol %). In particular, the higher replacing rates of the bulky -NO_2 and -SO_3H derivatives compared to the less hindered -H and -Me ones indeed highlight the key role of the electronic effect influence. It is noteworthy that dicarboxylic acids with heterocyclic five-membered rings could also substitute BTC efficiently (Table 1, entries 13-15, Figure S24). Especially the fact that 2,5-furan-dicarboxylic acid (FDC) shows notably higher ratio included (21 mol %) than that of the 2,5-thiophene-dicarboxylic acid (TDC) one (13 mol %) supports well the decisive role of electronic effect, since thiophene ring is well-known to be more electron-rich than furan is. In addition, the

substitution ligand could be extended to multicomponent with different functional groups. For instance, both IPA and 5-NO_2-IPA could be included in the MOF framework at the same time that further enriches the local chemical environment of the pore (Table 1, entry 16; Figure S24).

Linker substitution not only generates rich chemical environment of the cavity, but also displays pronounced effect on the surface area and pore volume of the MOF structure (Table 1, Figure S25-27 and Table S6). In comparison with the pure MIP-207, some secondary linkers could lead to a slight increase of the BET area and pore volume. For example, 5-NO_2-IPA substitution (entry 10) results in an increase of BET area up to 32% while introduction of TDC raises 54% the pore volume. However, some functional groups that might form strong binding with Ti(IV) ion decrease the surface area and pore content notably possibly due to the trapping of coordinated Ti complex impurities, as the case for 5-SO_3H-IPA (entry 11). The changes of BET area and pore volume for a given secondary linker case do not correlate to its steric hindrance, molecular weight and replacing ratio, which could be possibly explained by different linker defects.

It has been well-documented that the presence of polar functional group, such as -hydroxyl, -carboxyl and -amino, in the MOF structure could notably improve its carbon dioxide (CO_2) capture performance.[43-46] Nevertheless, it is very difficult to obtain Ti-MOFs with useful and accessible functional groups within the crystal framework. To date, only the NH_2-MIL-125[41; 47] containing free amino groups has been successfully synthesized as the analogue of MIL-125 despite its average performance in selective CO_2 adsorption probably due to the large open pore system of the framework and/or lack of strong adsorption sites. This fact somehow largely limits the possible application of Ti-MOFs in CO_2 separation and capture processes. As the first Ti-MOF with free carboxyl in the crystal structure, MIP-207 thus motivated us to investigate its performance in the application of selective CO_2 adsorption and separation.

Single component CO_2 and nitrogen (N_2) adsorption isotherms were collected on the MIP-207 sample to determine the CO_2 adsorption working capacity and calculated ideal adsorbed solution theory (IAST) selectivity of CO_2/N_2 for a typical post-combustion condition of Vacuum Swing Adsorption (VSA) process (CO_2/N_2=15/85, 298 K, 0.1-1 bar,

see SI). It is worthy to note that the desorption branch of CO_2 sorption isotherm is fully reversible for both temperatures (Figure 4a), indicating that regeneration of the MIP-207 sample could be realized under mild condition. Hence, the strong interaction with CO_2 and relatively small pore volume of the structure result in the CO_2 adsorptive uptake of MIP-207 at 298 K are 0.89 and 2.11 mmol g^{-1} for 0.15 bar and 1 bar, respectively, associated with an adsorptive working capacity of 0.63 mmol g^{-1}. To the best of our knowledge, these values are the highest among all the reported MOF structures with free carboxyl groups. Additionally, the calculated IAST selectivity is 52.8 and 81.2 for 298 K and 273 K separately when a binary gases mixture of CO_2:N_2=15:85 (v:v) was considered, which are evidently higher than that of all the other Ti-carboxylate MOFs and comparable with the one of MIL-91(Ti).

Furthermore, the adsorptive separation property of the MIP-207 framework on CO_2/N_2 could be easily adjusted by tuning the cavity chemical environment via secondary linker substitution (Figure 4b, Table 1, Figure S28). On one hand, it is of great interest to improve the working capacity while keeping the selectivity. For example, introduction of the pyridyl moiety by partially replacing BTC with 3,5-PYD could significantly enhance the working capacity to 0.84 mmol g^{-1} (33.3% increase) with a slightly increased IAST selectivity (Table 1, entry 12) in comparison with pure MIP-207. On the other hand, promotion in selectivity could be another aspect of interest. The highest IAST selectivity (60.7) among all the modified samples was achieved by inclusion a small amount of PDA, whose adjacent N/-NH- pair from the heterocyclic ring could possibly play an important role in enhancing the working capacity as well (entry 13). To confirm these results obtained by IAST, real coadoption measurements were performed with a homemade breakthrough apparatus (see supporting information) on the parent sample (MIP-207, Figure S30), the sample with the highest working capacity (MIP-207 substituted with 3,5-PYD, Figure S31) and the sample with the highest selectivity (MIP-207 substitutes with PDA, Figure S32). The experimental selectivity and working capacity values are in a very good agreement with those determined by IAST (Table S7). Therefore, MIP-207 provides a tunable scaffold regarding working capacity and selectivity for adsorptive separation of CO_2 over N_2.In summary, we report a controlled fabrication of a Ti-MOF (MIP-207) via direct synthesis applying a linker exchange and

installing strategy based on a Ti_8 cluster (Ti_8AF), in which the connection and configuration arrangement of the Ti_8 cluster precursor were kept. Due to the unique ditopic bonding mode of BTC linker, various IPA type secondary linkers with diverse functional groups have been introduced to the MOF framework and replaced BTC through concise one-pot reactions, allowing the rational adjustment of the tunable chemical environment of the MOF pore system. MIP-207 exhibits one of the best performance for CO_2/N_2 separation among all the reported Ti-carboxylate MOFs, with a good working capacity and an interesting selectivity of CO_2/N_2 under the typical post-combustion condition of CO_2/N_2=15/85, 298 K for a VSA process. As a result of the diverse chemical function involved from the substituted secondary linkers, further improvement of CO_2/N_2 separation performance of MIP-207 could be achieved easily. Moreover, both the Ti_8AF cluster precursor and MIP-207 feature scalable green syntheses and good air stabilities. Thus, MIP-207 represents the first Ti-MOF example that could be prepared over control under green scalable conditions. The wide tunability of the MOF pore environment and adequate stability of MIP-207 not only allow its good performance for CO_2/N_2 separation, but also provides encouraging possibility in other energy and environment related molecule separations.

EXPERIMENTAL PROCEDURES

MOFs syntheses

Reflux synthesis of Ti_8AF cluster. To a 500 mL round bottom flask, formic acid (200 mL), acetic anhydride (200 mL) and $Ti(iPrO)_4$ (40 mL) were added with stirring at room temperature (RT). The mixture was refluxed at 120°C for 12 hours. After cooled down to RT, the white crude product was collected by filtration or centrifuge. The final product was obtained by washing in boiling acetone and filtration or centrifuge. In order to keep the long-range order of the Ti_8AF cluster crystal structure for a long duration, immersion the product in acetone at RT is recommended. This procedure could be applied to either smaller scale or larger one upon the request of product quantity.

Solvothermal synthesis of MIP-207. To a 25 mL Teflon reactor, trimesic acid (BTC, 315 mg), acetic acid (2.5 mL), acetic anhydride (2.5 mL) were added and stirred at RT. $Ti(iPrO)_4$ (300 µL) was added last while stirring. The reaction mixture was sealed in an

autoclave and was heated at 120°C for 48 hours. After cooled down to RT, the crude product was collected by filtration, followed by washing it in boiling acetone for activation. The final product was obtained by filtration and air-dry.

Reflux synthesis of MIP-207. To a 250 mL round bottom flask, BTC (4.2 g), acetic acid (50 mL) and acetic anhydride (50 mL) were added and mixed at RT. $Ti(iPrO)_4$ (4 mL) was added last while stirring. The reaction mixture was refluxed at 120°C for 12 hours. After cooled down to RT, the crude product was collected by filtration, followed by washing it in boiling acetone for activation. The final product was obtained by filtration and air-dry. This procedure could be applied to either smaller scale or larger one upon the request of product quantity.

Synthesis of substituted MIP-207 with secondary linkers with different functional groups. To a 50 mL round bottom flask, BTC (630 mg, 3 mmol), secondary linker (1 mmol), acetic acid (10 mL) and acetic anhydride (10 mL) were added and mixed at RT. $Ti(iPrO)_4$ (800 µL) was added last while stirring. The reaction mixture was refluxed at 120°C for 12 hours. After cooled down to RT, the crude product was collected by filtration, followed by washing it in boiling acetone for activation. The final product was obtained by filtration and air-dry.

Co-adsorption breakthrough measurement

The co-adsorption breakthrough curves are measured with a homemade device (Figure S29). It is mainly composed of an adsorption column (5 cm height and 1 cm diameter (Volume: 3.9 cm^3)) placed in an oven, a gas supply system with two mass flow controllers [MFC] (one for helium and one for N_2/CO_2 mixture) and a mass spectrometer to analyze gas composition at the outlet of the column.

Prior to each measurement, the adsorbent is outgassed at 423K in the oven for 12 hours under secondary vacuum. After cooling to 298K, a helium flow is set to 2Nl/h to pressurize the column. The breakthrough curve measurement is started by switching helium flow to N_2/CO_2 mixture (85/15) flow of 1Nl/h (minimum set point value). The resulting pressure is 1.2 bar. the measurements are repeated twice (Run 1 and Run 2) for each sample.

AKNOWLEDGEMENT

The authors are grateful to the ANR Project MeaCoPA (ANR-17-CE29-0003) for financial support.

AUTHOR CONTRIBUTIONS

Conceptualization, S.W. and C.S.; Investigation, S.W., H.R., N.H., M.W., C.M., G.D.W. and G.M.; Writing-Original Draft, S.W.; Writing-Review & Editing, S.W. H.R., N.H., M.W., C.M., G.D.W., G.M. and C.S. Supervision, G.D.W., G.M. and C.S.

DECLARATION OF INTEREST

The authors declare no competing interest.

REFERENCES

1. Zhu J. J., Li P. Z., Guo W. H., Zhao Y. L., and Zou R. Q. (2018). Titanium-based metal-organic frameworks for photocatalytic applications. Coord Chem Rev *359*, 80-101.
2. Dolgopolova E. A., Rice A. M., Martin C. R., and Shustova N. B. (2018). Photochemistry and photophysics of MOFs: steps towards MOF-based sensing enhancements. Chem Soc Rev *47*, 4710-4728.
3. Horiuchi Y., Toyao T., Saito M., Mochizuki K., Iwata M., Higashimura H., et al. (2012). Visible-Light-Promoted Photocatalytic Hydrogen Production by Using an Amino-Functionalized Ti(IV) Metal-Organic Framework. J Phys Chem C *116*, 20848-20853.
4. Fu Y., Sun D., Chen Y., Huang R., Ding Z., Fu X., et al. (2012). An Amine-Functionalized Titanium Metal–Organic Framework Photocatalyst with Visible-Light-Induced Activity for CO2 Reduction. Angew ChemInt Ed *51*, 3364-3367.
5. Benoit V., Pillai R. S., Orsi A., Normand P., Jobic H., Nouar F., et al. (2016). MIL-91(Ti), a small pore metal–organic framework which fulfils several criteria: an upscaled green synthesis, excellent water stability, high CO2 selectivity and fast CO2 transport. J Mater Chem A *4*, 1383-1389.
6. Sun Y., Liu Y., Caro J., Guo X., Song C., and Liu Y. (2018). In-Plane Epitaxial Growth of Highly c-Oriented NH2-MIL-125(Ti) Membranes with Superior H2/CO2 Selectivity. Angew ChemInt Ed *57*, 16088-16093.
7. Serre C., Groves J. A., Lightfoot P., Slawin A. M. Z., Wright P. A., Stock N., et al. (2006). Synthesis, Structure and Properties of Related MicroporousN,N'-Piperazinebismethylenephosphonates of Aluminum and Titanium. Chem Mat *18*, 1451-1457.

8. Dan-Hardi M., Serre C., Frot T., Rozes L., Maurin G., Sanchez C., et al. (2009). A new photoactive crystalline highly porous titanium(IV) dicarboxylate. J Am Chem Soc *131*, 10857-10859.
9. Gao J., Miao J., Li P.-Z., Teng W. Y., Yang L., Zhao Y., et al. (2014). A p-type Ti(iv)-based metal–organic framework with visible-light photo-response. Chem Commun *50*, 3786-3788.
10. Mason J. A., Darago L. E., Lukens W. W., Jr., and Long J. R. (2015). Synthesis and O2 Reactivity of a Titanium(III) Metal-Organic Framework. Inorg Chem *54*, 10096-10104.
11. Bueken B., Vermoortele F., Vanpoucke D. E., Reinsch H., Tsou C. C., Valvekens P., et al. (2015). A Flexible Photoactive Titanium Metal-Organic Framework Based on a [Ti(IV)3(mu3-O)(O)2(COO)6] Cluster. Angew ChemInt Ed *54*, 13912-13917.
12. Nguyen N. T., Furukawa H., Gandara F., Trickett C. A., Jeong H. M., Cordova K. E., et al. (2015). Three-Dimensional Metal-Catecholate Frameworks and Their Ultrahigh Proton Conductivity. J Am Chem Soc *137*, 15394-15397.
13. Assi H., Pardo Perez L. C., Mouchaham G., Ragon F., Nasalevich M., Guillou N., et al. (2016). Investigating the Case of Titanium(IV) Carboxyphenolate Photoactive Coordination Polymers. Inorg Chem *55*, 7192-7199.
14. Wang S., Kitao T., Guillou N., Wahiduzzaman M., Martineau-Corcos C., Nouar F., et al. (2018). A phase transformable ultrastable titanium-carboxylate framework for photoconduction. Nat Commun *9*, 1660.
15. Castells-Gil J., M. Padial N., Almora-Barrios N., da Silva I., Mateo D., Albero J., et al. (2019). De novo synthesis of mesoporous photoactive titanium(iv)–organic frameworks with MIL-100 topology. Chem Sci *10*, 4313-4321.
16. Lan G., Ni K., Veroneau S. S., Feng X., Nash G. T., Luo T., et al. (2019). Titanium-Based Nanoscale Metal–Organic Framework for Type I Photodynamic Therapy. J Am Chem Soc *141*, 4204-4208.
17. Li C., Xu H., Gao J., Du W., Shangguan L., Zhang X., et al. (2019). Tunable titanium metal–organic frameworks with infinite 1D Ti–O rods for efficient visible-light-driven photocatalytic H2 evolution. J Mater Chem A *7*, 11928-11933.
18. Kim M., Cahill J. F., Fei H., Prather K. A., and Cohen S. M. (2012). Postsynthetic Ligand and Cation Exchange in Robust Metal–Organic Frameworks. J Am Chem Soc *134*, 18082-18088.
19. Brozek C. K., and Dinca M. (2013). Ti(3+)-, V(2+/3+)-, Cr(2+/3+)-, Mn(2+)-, and Fe(2+)-substituted MOF-5 and redox reactivity in Cr- and Fe-MOF-5. J Am Chem Soc *135*, 12886-12891.
20. Zou L., Feng D., Liu T.-F., Chen Y.-P., Yuan S., Wang K., et al. (2016). A versatile synthetic route for the preparation of titanium metal–organic frameworks. Chem Sci *7*, 1063-1069.
21. Yuan S., Liu T.-F., Feng D., Tian J., Wang K., Qin J., et al. (2015). A single crystalline porphyrinic titanium metal–organic framework. Chem Sci *6*, 3926-3930.
22. Nguyen H. L., Gándara F., Furukawa H., Doan T. L. H., Cordova K. E., and Yaghi O. M. (2016). A Titanium–Organic Framework as an Exemplar of Combining the Chemistry of Metal– and Covalent–Organic Frameworks. J Am Chem Soc *138*, 4330-4333.
23. Nguyen H. L., Vu T. T., Le D., Doan T. L. H., Nguyen V. Q., and Phan N. T. S. (2017). A Titanium–Organic Framework: Engineering of the Band-Gap Energy for Photocatalytic Property Enhancement. ACS Catal *7*, 338-342.
24. Surblé S., Serre C., Mellot-Draznieks C., Millange F., and Férey G. (2006). A new isoreticular class of metal-organic-frameworks with the MIL-88 topology. Chem Commun, 284-286.
25. Dybtsev D. N., Sapianik A. A., and Fedin V. P. (2017). Pre-synthesized secondary building units in the rational synthesis of porous coordination polymers. Mendeleev Commun *27*, 321-331.
26. Peng L., Asgari M., Mieville P., Schouwink P., Bulut S., Sun D. T., et al. (2017). Using Predefined M3(μ3-O) Clusters as Building Blocks for an Isostructural Series of Metal–Organic Frameworks. ACS Appl Mater Interfaces *9*, 23957-23966.

27. DeStefano M. R., Islamoglu T., Garibay S. J., Hupp J. T., and Farha O. K. (2017). Room-Temperature Synthesis of UiO-66 and Thermal Modulation of Densities of Defect Sites. Chem Mat *29*, 1357-1361.
28. Noh H., Kung C.-W., Islamoglu T., Peters A. W., Liao Y., Li P., et al. (2018). Room Temperature Synthesis of an 8-Connected Zr-Based Metal–Organic Framework for Top-Down Nanoparticle Encapsulation. Chem Mat *30*, 2193-2197.
29. Guillerm V., Gross S., Serre C., Devic T., Bauer M., and Férey G. (2010). A zirconium methacrylate oxocluster as precursor for the low-temperature synthesis of porous zirconium(iv) dicarboxylates. Chem Commun *46*, 767-769.
30. Keum Y., Park S., Chen Y.-P., and Park J. (2018). Titanium-Carboxylate Metal-Organic Framework Based on an Unprecedented Ti-Oxo Chain Cluster. Angew ChemInt Ed *57*, 14852-14856.
31. Feng X., Song Y., Chen J. S., Li Z., Chen E. Y., Kaufmann M., et al. (2019). Cobalt-bridged secondary building units in a titanium metal–organic framework catalyze cascade reduction of N-heteroarenes. Chem Sci *10*, 2193-2198.
32. Steunou N., Robert F., Boubekeur K., Ribot F., and Sanchez C. (1998). Synthesis through an in situ esterification process and characterization of oxo isopropoxo titanium clusters. Inorg Chim Acta *279*, 144-151.
33. Rozes L., and Sanchez C. (2011). Titanium oxo-clusters: precursors for a Lego-like construction of nanostructured hybrid materials. Chem Soc Rev *40*, 1006-1030.
34. Assi H., Mouchaham G., Steunou N., Devic T., and Serre C. (2017). Titanium coordination compounds: from discrete metal complexes to metal–organic frameworks. Chem Soc Rev *46*, 3431-3452.
35. Fang W.-H., Zhang L., and Zhang J. (2018). Synthetic strategies, diverse structures and tuneable properties of polyoxo-titanium clusters. Chem Soc Rev *47*, 404-421.
36. Chakraborty B., and Weinstock I. A. (2019). Water-soluble titanium-oxides: Complexes, clusters and nanocrystals. Coord Chem Rev *382*, 85-102.
37. Wu H., Chua Y. S., Krungleviciute V., Tyagi M., Chen P., Yildirim T., et al. (2013). Unusual and Highly Tunable Missing-Linker Defects in Zirconium Metal–Organic Framework UiO-66 and Their Important Effects on Gas Adsorption. J Am Chem Soc *135*, 10525-10532.
38. Schaate A., Roy P., Godt A., Lippke J., Waltz F., Wiebcke M., et al. (2011). Modulated Synthesis of Zr-Based Metal–Organic Frameworks: From Nano to Single Crystals. Chem Euro J *17*, 6643-6651.
39. Bai Y., Dou Y., Xie L. H., Rutledge W., Li J. R., and Zhou H. C. (2016). Zr-based metal-organic frameworks: design, synthesis, structure, and applications. Chem Soc Rev *45*, 2327-2367.
40. Wang S., Lee J. S., Wahiduzzaman M., Park J., Muschi M., Martineau-Corcos C., et al. (2018). A robust large-pore zirconium carboxylate metal–organic framework for energy-efficient water-sorption-driven refrigeration. Nat Energy *3*, 985-993.
41. Gordeeva L. G., Solovyeva M. V., and Aristov Y. I. (2016). NH2-MIL-125 as a promising material for adsorptive heat transformation and storage. Energy *100*, 18-24.
42. Permyakova A., Wang S., Courbon E., Nouar F., Heymans N., D'Ans P., et al. (2017). Design of salt–metal organic framework composites for seasonal heat storage applications. J Mater Chem A *5*, 12889-12898.
43. Trickett C. A., Helal A., Al-Maythalony B. A., Yamani Z. H., Cordova K. E., and Yaghi O. M. (2017). The chemistry of metal–organic frameworks for CO2 capture, regeneration and conversion. Nat Rev Mater *2*, 17045.
44. Liu J., Thallapally P. K., McGrail B. P., Brown D. R., and Liu J. (2012). Progress in adsorption-based CO2 capture by metal–organic frameworks. Chem Soc Rev *41*, 2308-2322.
45. González-Zamora E., and Ibarra I. A. (2017). CO2 capture under humid conditions in metal–organic frameworks. Mater Chem Front *1*, 1471-1484.

46. Hu Z., Zhang K., Zhang M., Guo Z., Jiang J., and Zhao D. (2014). A Combinatorial Approach towards Water-Stable Metal–Organic Frameworks for Highly Efficient Carbon Dioxide Separation. ChemSusChem *7*, 2791-2795.
47. Hendon C. H., Tiana D., Fontecave M., Sanchez C., D'Arras L., Sassoye C., et al. (2013). Engineering the optical response of the titanium-MIL-125 metal-organic framework through ligand functionalization. J Am Chem Soc *135*, 10942-10945.

Figure legends

Figure 1. Comparison of some Ti_8 clusters reported with protection ligands of (A) 4-aminobenzoic acid, (B) sulfate, (C) a phosphorous acid derivative, (D) isobutyric acid, (E) terephthalic acid and (F) the Ti_8AF in this work. Ti in blue, C in gray, O in red, S in yellow and P in pink.

Figure 2. Crystal structure of MIP-207. (A) A $Ti_8(\mu_2\text{-}O)_8(acetate)_8(BTC)_4$ cluster SBU. (B) A single 2D layer viewed along the *c*-axis. (C) Micropore system viewed along the *c*-axis. (D) Adjacent 2D layers closely packed with a large amount of guest water molecules in between to stabilize the crystal structure. Ti in light blue, C in gray and O in red.

Figure 3. (A) Illustration of linker substitution in MIP-207 crystal structure, the functional isophthalate type linkers are marked with colors. (B) Linker substitution ratio determined by ^1H NMR data collected with the decomposed MOF samples in D_2O/KOH solution. Standard condition for all the reactions involving mixed linkers: $Ti(iPrO)_4$ (3 mmol), BTC (3 mmol), secondary linker (1 mmol), acetic acid (10 mL), acetic anhydride (10 mL), reflux overnight.

Figure 4. (A) CO_2 and N_2 sorption isotherms of MIP-207 collected at 273 K and 298 K separately. (B) Comparison of IAST selectivity (CO_2:N_2=15:85 v:v, 298 K, 1 bar) and CO_2 adsorption working capacity (CO_2:N_2=15:85 v:v, 298 K, 0.1-1 bar) between MIP-207 and samples with different substituted linkers.

Table 1. Summary of secondary linker substitution and corresponding selective CO_2 sorption performance.

entry	substitution linker	ratio[a] (mol %)	S_{BET}[b] (m^2 g^{-1})	S_{BET}[b] (m^2 cm^{-3})	CO_2 uptake 298 K 0.15 bar (mmol g^{-1})	CO_2 working capacity 298 K (mmol g^{-1})	CO_2 working capacity 298 K (µmol g^{-1} m^{-2})	IAST selectivity CO_2:N_2=15:85 298 K/1 bar
1	-	-	590	820	0.89	0.63	1.07	52.8
2	5-tBu-IPA	5	680	950	0.88	0.63	0.93	45.2
3	5-OH-IPA	7	530	740	0.69	0.52	0.98	42.3
4	5-Me-IPA	7	750	1040	1.04	0.73	0.97	55.5
5	5-NH_2-IPA	7	630	880	1.00	0.71	1.13	48.4
6	IPA	8	670	930	0.82	0.60	0.90	45.7
7	5-OMe-IPA	9	750	1040	1.01	0.71	0.95	47.8
8	5-F-IPA	12	560	780	0.86	0.61	1.09	50.8
9	5-Br-IPA	12	620	870	0.85	0.61	0.98	48.6
10	5-NO_2-IPA	13	780	1090	0.81	0.59	0.76	47.3
11	5-SO_3H-IPA	17	420	590	0.52	0.43	1.02	27.2
12	3,5-PYD[c]	18	680	930	1.21	0.84	1.24	53.6
13	PDA[d]	5	730	1010	1.14	0.79	1.08	60.7
14	TDC[e]	13	770	1060	1.09	0.75	0.97	58.3
15	FDC[f]	21	750	1020	1.02	0.72	0.96	49.2
16	IPA 5-NO_2-IPA	5 5	680	940	0.96	0.69	1.01	43.0

[a]The ratio of the secondary linker was determined by the NMR data obtained with decomposed MOF product in D_2O/KOH solution. [b]Data obtained from the nitrogen adsorption isotherm collected at 77 K. [c]3,5-pyridine-dicarboxylic acid. [d]3,5-pyrazole-dicarboxylic acid. [e]2,5-thiophene-dicarboxylic acid. [f]2,5-furan-dicarboxylic acid.

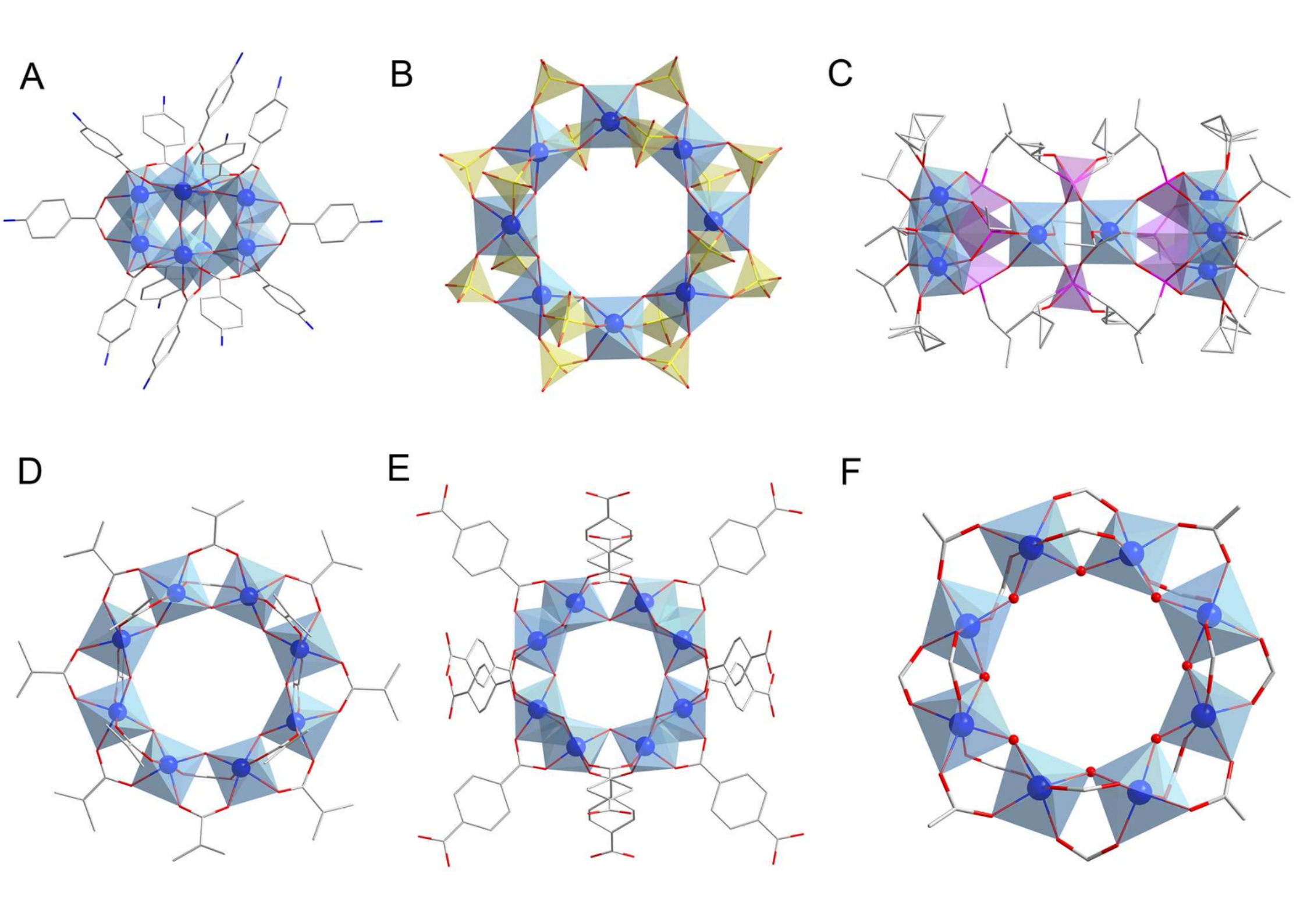
A
B
C
D
E
F

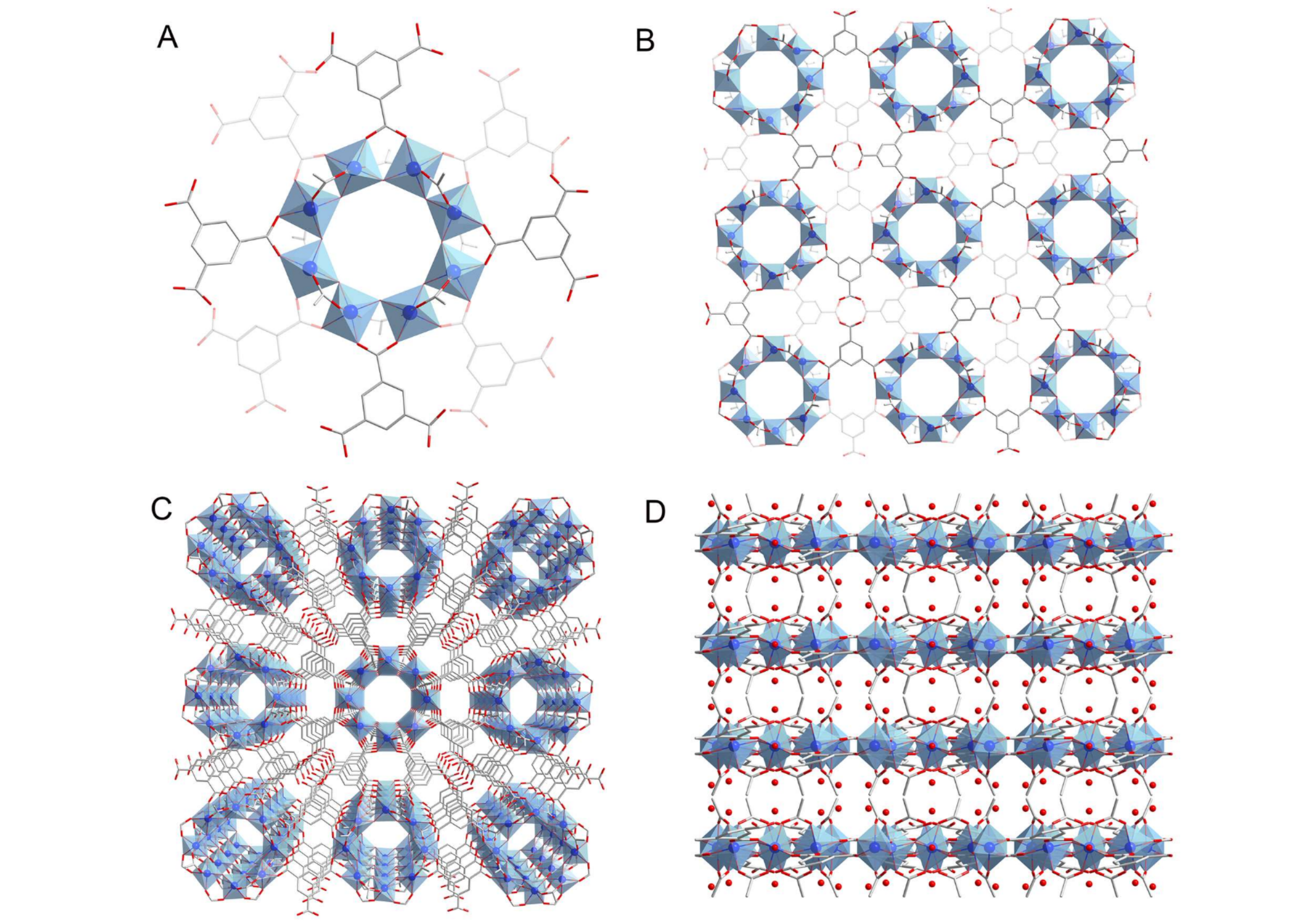
A
B
C
D

A

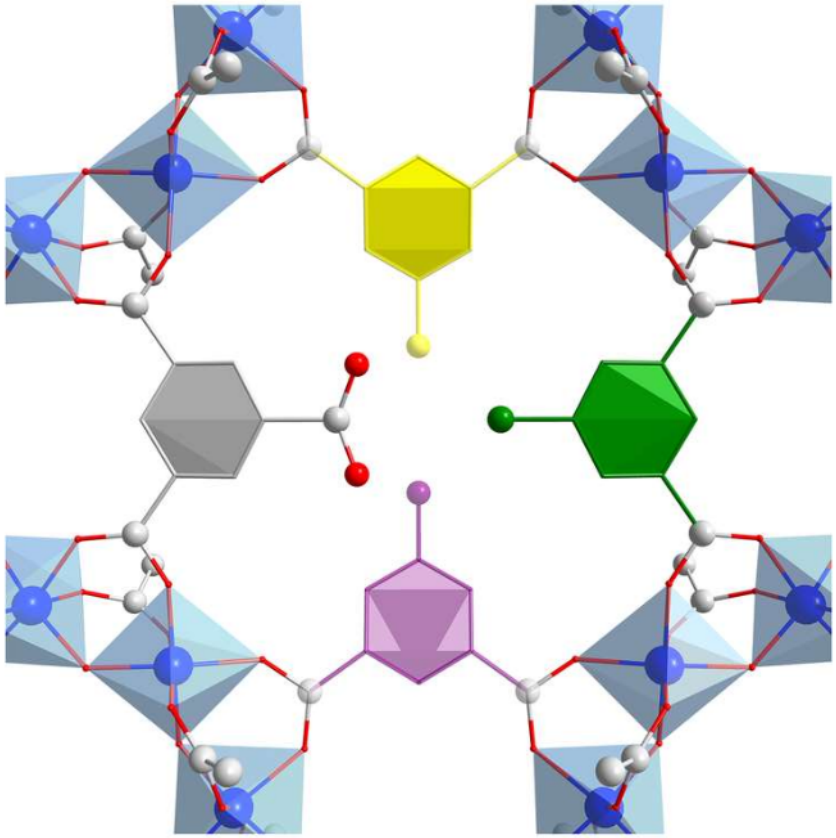

B

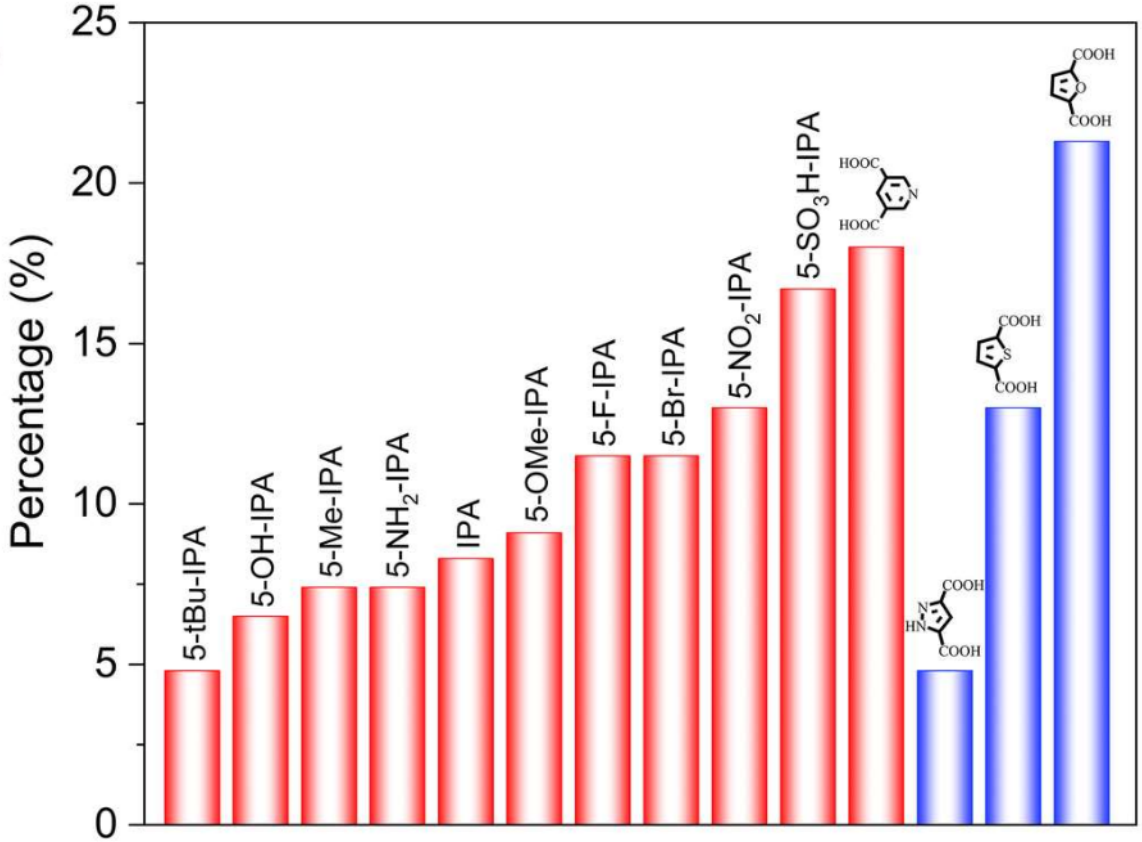
Percentage (%)
0
5
10
15
20
25
5-tBu-IPA
5-OH-IPA
5-Me-IPA
5-NH2-IPA
IPA
5-OMe-IPA
5-F-IPA
5-Br-IPA
5-NO2-IPA
5-SO3H-IPA
HOOC
HOOC
N
COOH
HN
N
COOH
COOH
COOH
S
COOH
COOH
O
COOH

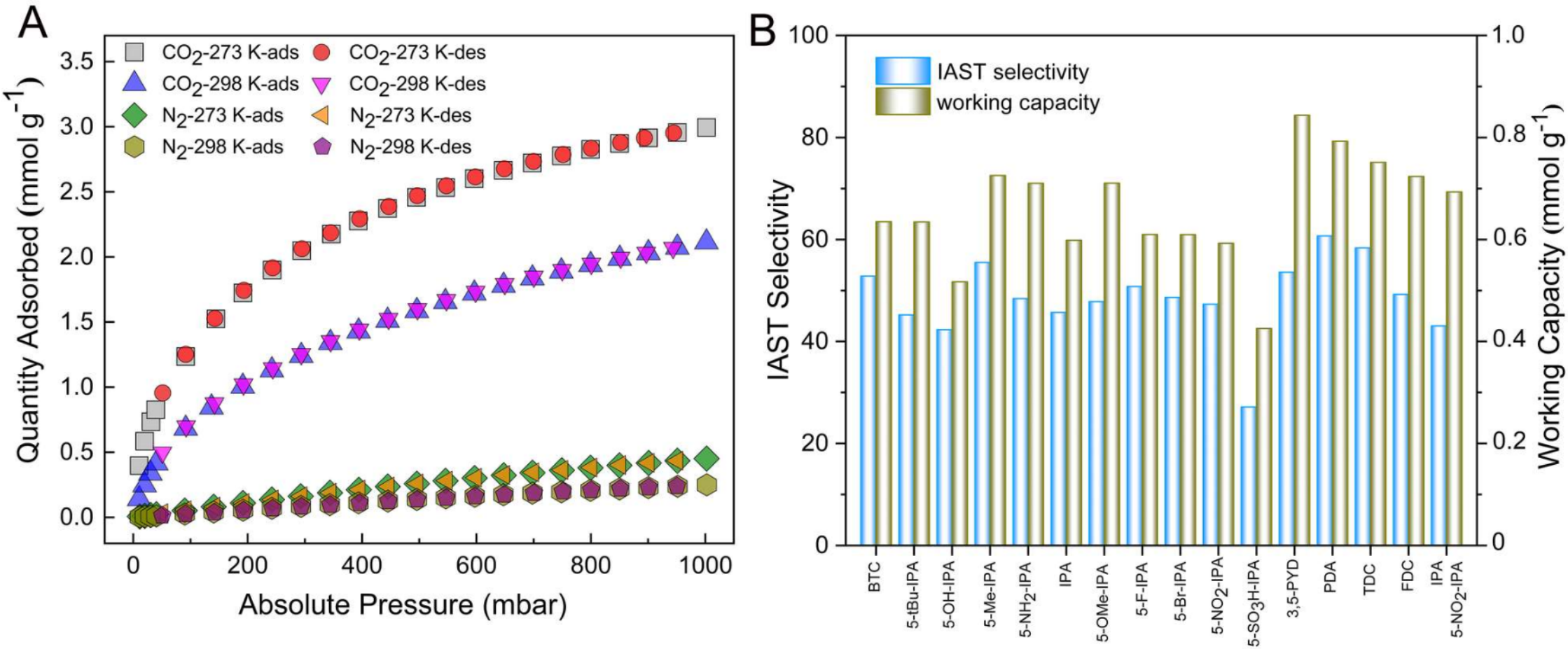
A
CO2-273 K-ads
CO2-273 K-des
CO2-298 K-ads
CO2-298 K-des
N2-273 K-ads
N2-273 K-des
N2-298 K-ads
N2-298 K-des
Quantity Adsorbed (mmol g-1)
Absolute Pressure (mbar)
B
IAST selectivity
working capacity
IAST Selectivity
Working Capacity (mmol g-1)
BTC
5-tBu-IPA
5-OH-IPA
5-Me-IPA
5-NH2-IPA
IPA
5-OMe-IPA
5-F-IPA
5-Br-IPA
5-NO2-IPA
5-SO3H-IPA
3,5-PYD
PDA
TDC
FDC
IPA
5-NO2-IPA

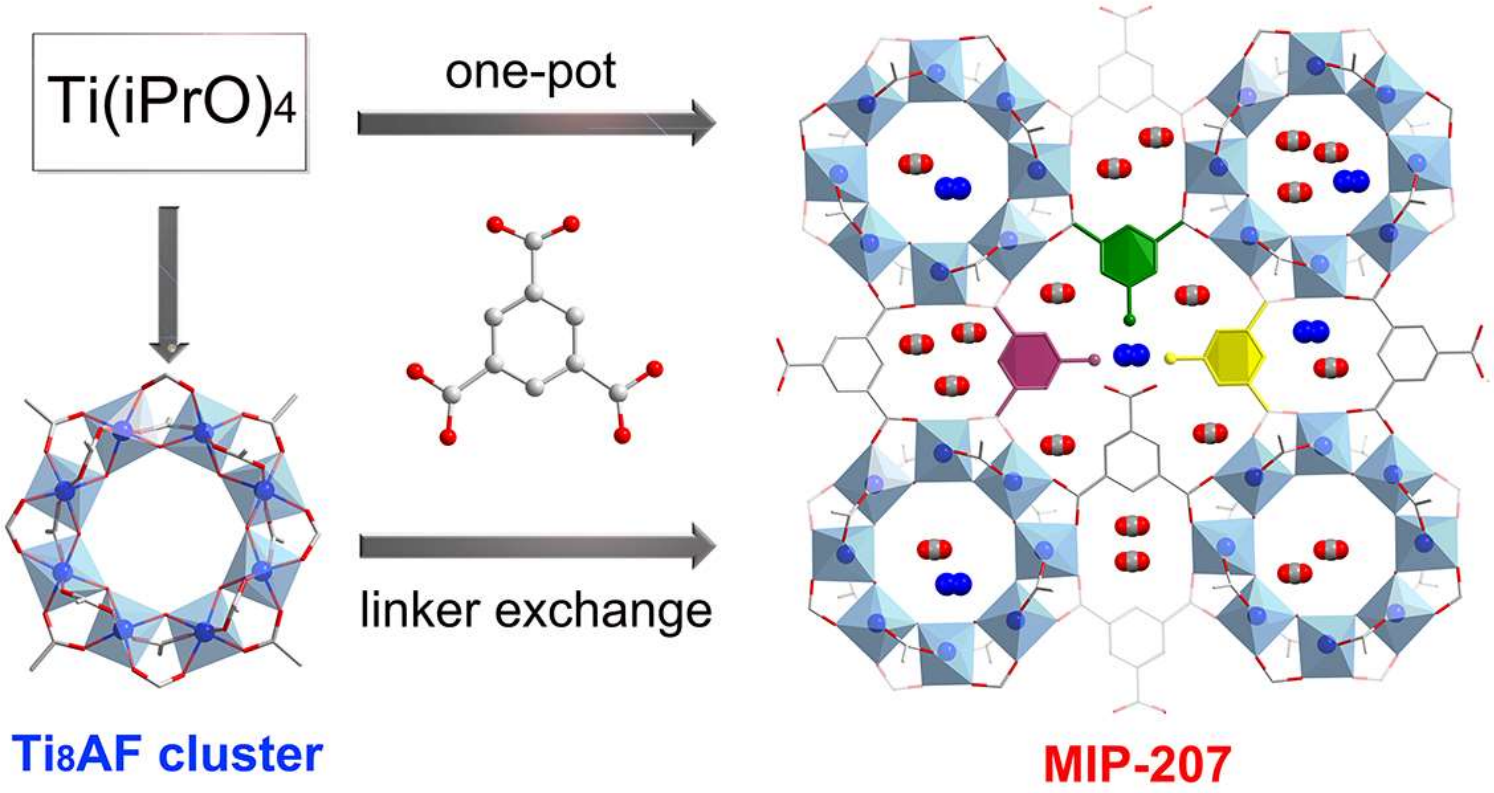
Ti(iPrO)4
one-pot
linker exchange
Ti8AF cluster
MIP-207

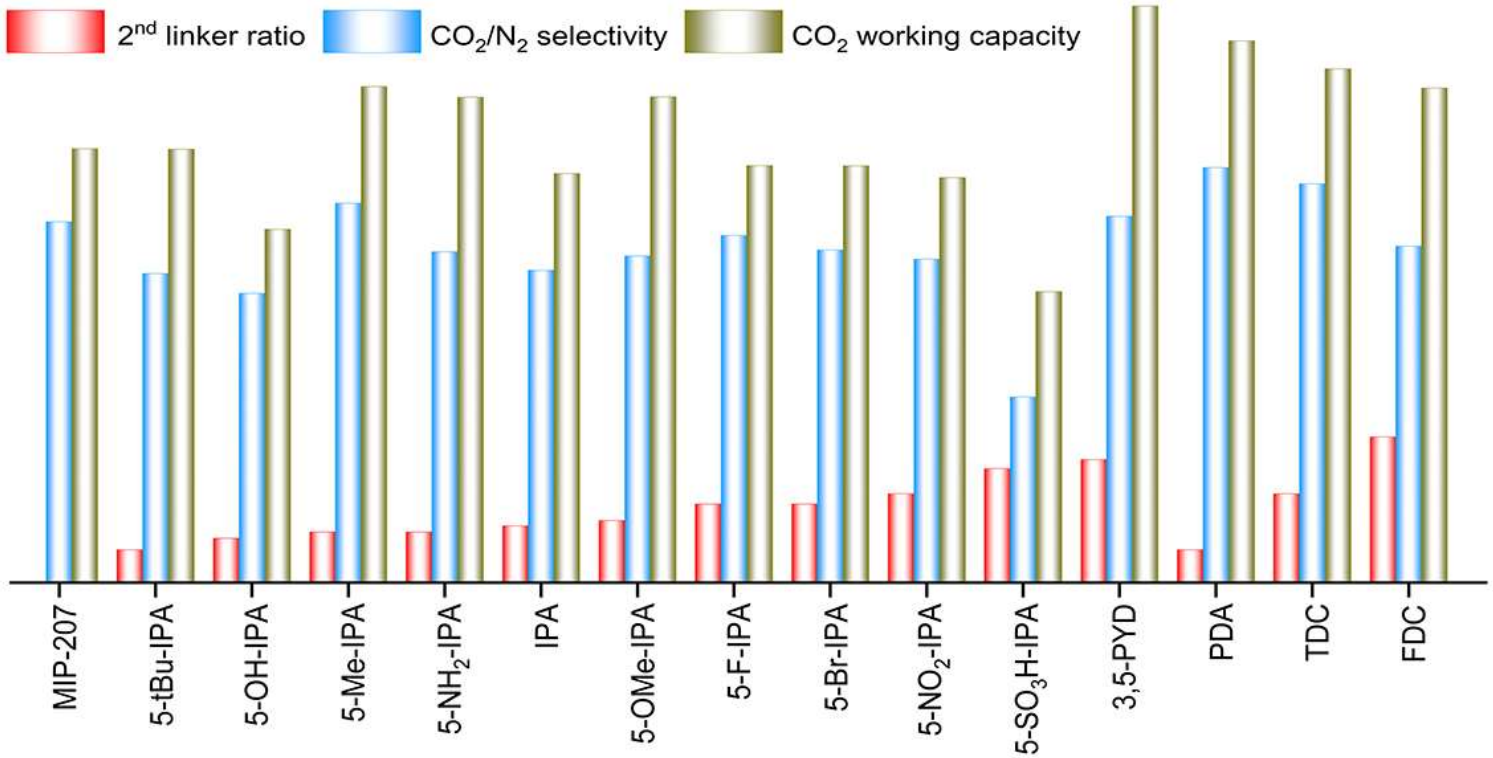
2nd linker ratio
CO2/N2 selectivity
CO2 working capacity
MIP-207
5-tBu-IPA
5-OH-IPA
5-Me-IPA
5-NH2-IPA
IPA
5-OMe-IPA
5-F-IPA
5-Br-IPA
5-NO2-IPA
5-SO3H-IPA
3,5-PYD
PDA
TDC
FDC